Desalination and Water Treatment
www.deswater.com

doi: 10.5004/dwt.2017.21384

89 (2017) 65–76
September

Solar-driven dual-purpose plant with hybrid desalination system for harsh desert farms

Ashraf Sadik Hassan[a,*], Hassan Elbanna Fath[b]

[a]*Qatar Environment and Energy Research Institute, Hamad Bin Khalifa University, Doha, Qatar, email: ahassan@hbku.edu.qa*
[b]*Egypt-Japan University of Science and Technology (E-JUST), Alexandria, Egypt, email: h_elbanna_f@yahoo.com*

Received 18 April 207; Accepted 25 August 2017

ABSTRACT

This work presents the process design and operational performance of a small-scale solar-driven dual-purpose plant to generate electricity and produce desalinated freshwater. The plant consists of a hybrid desalination system of reverse osmosis (RO) and a vacuum multi-effect membrane distillation (V-MEMD), coupled with a solar linear Fresnel collector (LFC) and a turbo-generator system. The integrated system is designed to provide the optimum solution for big desert farms of high groundwater salinity (of 15,000 ppm and more). The RO is designed with 40% recovery and its brine is used to feed V-MEMD units of almost the same recovery of around 40%. The system (base case) is designed with turbo-generator to provide the plant and the farm with electrical power (rating 68 kW) while the hybrid desalination plant is designed with 617 m^3/d capacity. Other scale up designs for electricity and water production will also be highlighted. The technical analysis of the dual-purpose system will be presented including; the plant specifications, process design and components sizing parameters of hybrid desalination plant and solar LFC.

Keywords: Reverse osmosis; Multi-effect vacuum membrane distillation; Solar leaner Fresnel collector; Dual-purpose plant; Hybrid desalination system

1. Introduction

Although Qatar is a small population country (2,576,181 in January 2017), it is among the highest in the world regarding per capita water consumption. The available groundwater is also very limited with gradual increase in its salinity. For remote areas, provision of both freshwater and electricity present a real challenge for both Qatar and Egypt and for other world countries.

Water is an extremely scarce resource in the Gulf Cooperation Council (GCC) countries, which is one of the world's most arid regions. With only limited groundwater resources, and amid growing signs that groundwater is being depleted by over-use, the GCC countries are facing potential severe water shortages. The next years, Qatar for example, will face rising water demand, as the expanding middle class adopts an increasingly water-intensive lifestyle, featuring private swimming pools, gardens requiring big sprinkler systems, and even a growing interest in golf sport. Over the next decade, GCC countries will be among the world's highest per-capita users of water (Fig. 1) [1]. Although the economic forecast is positive, it carries a risk: that unmanaged growth will bring negative side-effects such as power shortages and soaring prices, in particular for food. Some GCC countries are already experiencing sporadic shortages of electricity and gas, while water supplies are already strained and food shortages loom as risks for an import-dependent region. A key challenge for the Gulf in the next decade will be to manage energy, water and food resources to ensure both high living standards and sustainable growth in the long-term. Aware of these challenges, Gulf Arab countries are undertaking a variety of measures to ensure long-term sustainable growth. These include [1]:

- Introducing energy-efficiency measures;
- Investing in clean fuel and renewable energy supplies;
- Improving water systems efficiency;

* Corresponding author.

- Investing in new water desalination capacity; and
- Buying or leasing agricultural land abroad.

Qatar is a small country in terms of population, but it is one of the world's largest water consumers on a per capita basis. As shown in Fig. 2, more than half of the country's water goes to the agricultural sector, but increasing demand is coming from the country's growing urban population. It is a country with limited and declining groundwater resources, and the country is therefore investing heavily in desalination plants. It has one of the longest-standing desalination programs in the Middle East. Therefore, there is a need for an efficient, cost-effective real system that can generate electricity and produce potable water using waste or renewable heat sources thus reducing energy consumption and CO_2 emissions [2]. Qatar's groundwater aquifers may serve as valuable reservoirs and feedwater sources to help minimizing the current dependence of seawater desalination. The current practice of direct irrigation is resulting in soil salinization and desertification across the country. Kuiper et al. [3] indicated that similar to other arid nations, Qatar's aquifers are highly susceptible to contamination due to overexploitation and rapid industrialization creating conditions of vulnerability for local environments and populations. Groundwater in Qatar was brackish to saline (25th–75th percentile total dissolved solid [TDS] = 2,140–4,660 mg/L); sodium absorption ratio (mean = 10.1) and electric conductivity (mean = 7,250 μS/cm) values indicate continued use of Qatar's groundwater for irrigation may compromise soil structure and crop yield. Physicochemical properties and cation, anion and trace element content of Qatar's groundwater were quantified and potential contaminant sources and inter-element correlations have been explored. It has been compared with domestic and international regulatory standards and guideline values for drinking and irrigation water to determine suitability for current and potential uses, as shown in Table 1.

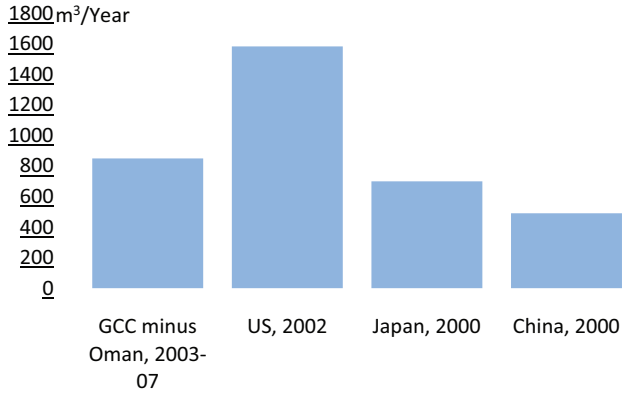

Fig. 1. Average water consumption per head in GCC and other regions, m^3/year [1].

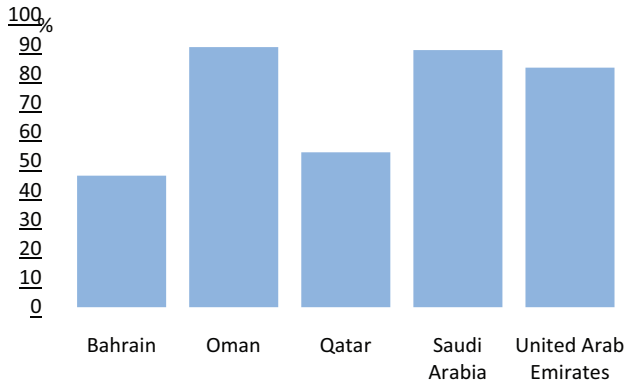

Fig. 2. Agriculture use of water in GCC countries as percentage of total consumption, 2003–2007 [1].

2. Solar thermal systems

The concentrating solar power (CSP) is the main market available technologies to utilize solar thermal energy. CSP system uses mirrors or lenses to concentrate solar energy and then employs a heat transfer fluid (HTF) or steam generated then transport the steam to turbines for power production or as thermal energy supply. For current CSP systems, the water requirement is estimated between 3 and 3.5 m^3/kW h, 95% of which is attributed to cooling tower and 5% is consumed for mirror cleaning [4,5]. Fig. 3 shows the direct normal irradiation on Qatar land, which the amount of the average solar radiation direction of the sun measured between 1,650 and 1,850 kWh/m^2/year [6]. On the other hand, solar collectors are usually classified into two categories according to concentration ratios [7]: non-concentrating collectors and concentrating collectors. A non-concentrating collector has the same intercepting area as its absorbing area, while a sun-tracking concentrating solar collector usually has concave reflecting surfaces to intercept and focus the solar irradiation to a much smaller receiving area, resulting in an increased heat flux so that the thermodynamic cycle can achieve higher Carnot efficiency (when working under higher temperatures). CSP technology dates back to 1970s, but most of the commercial CSP installations were made in the last decade particularly in Spain and USA. Four commonly used types of CSP technology are shown in Fig. 4; parabolic trough collector (PTC), linear Fresnel collector (LFC), solar power tower (SPT) and parabolic dish systems (PDS). PTC and LFR are line-focused technologies focusing the sun light to a line of receivers typically oriented in the north–south direction, whereas SPT and PDS are point-focused technologies focusing the sun light to a point where the receiver is located. Currently, PTC occupies more than 82% of the global CSP installations.

However, most recent CSP installations in USA, including the world's largest CSP plant Ivanpah SPT commissioned in 2014 (Ivanpah Dry Lake, CA), are SPT systems. The main reason for the present trend of installing SPT systems is the potential enhancement in efficiency of converting heat into electricity with SPT, and is also more suitable for achieving very high temperatures. The only disadvantage of SPT is that the initial installation cost is high compared with other CSP technologies [4]. Table 2 shows more details about the commercial maturity and other characteristics of all the CSP technologies. The table shows why LFC is selected in this study; as it has low relative cost, low operating temperature conditions, high power capacity range and it can be built as modular units. Table 3 shows the thermophysical properties the commercial figure of different types of HTFs, which the cost the water/steam is almost zero. CSP can play a major role

Table 1
Groundwater physical parameters, anions, cations and trace element concentrations compared with local and international standards for water use in Doha [3]

Parameter	Mean	Minimum	Maximum	FAO[a]	USEPA[b]	WHO[c]	GSO[d]
pH	7.81	6.94	8.22	6.5–8.4	–	–	–
Electrical conductivity, μS/cm	7,250	22.0	30,600	<700[e] 700–3,000[f] >3,000[g]	–	–	–
TDS, mg/L	3,553	11.0	14,959	<450[e] 450–2,000[f] >2,000[g]	–	–	–
Sodium absorption ratio	10.1	0.35	35.4	<10[e] 10–10[f] >18[g]	–	–	–
Br, mg/L	2.59	0.03	26.0	–	–	–	–
Cl, mg/L	1,540	9.5	9,560	<142[e] 142–355[f] >355[g]	4.0	5.0	50
F, mg/L	1.88	0.46	4.55	1.0	4.0	1.5	1.5
NO_3, mg/L	23.6	0.15	389	<5[e] 5–30[f] >30[g]	10.0	50	50
SO_4, mg/L	1,330	3.6	3,240	–	–	–	–
HCO_3^-, mg/L	30.8	1.06	63.0	<130.5[e] 130.5–740[f] >740[g]	–	–	–
Total organic carbon, mg/L	4.59	1.51	28.9	–	–	–	–
Ca, mg/L	346	4.11	985	–	–	–	–
K, mg/L	62.7	0.45	263	–	–	–	–
Mg, mg/L	127	2.75	610	–	–	–	–
Na, mg/L	923	6.9	5,500	<69[e] 69–207[f] >207[d]	–	–	–
As, μg/L	2.55	0.03	71.6	100	10	10	10
Ba, μg/L	26.3	1.74	139	–	2,000	700	700
Cd, μg/L	0.312	0.05	8.67	10	5	3	3
Co, μg/L	0.139	<0.017[h]	2.46	50	–	–	–
Cr, μg/L	2.5	0.1	15.7	100	100	50	50
Cu, μg/L	4.36	<0.12[h]	288	200	1,300	2,000	1,000
Fe, μg/L	55.8	2.37	1,900	5,000	–	–	–
Mn, μg/L	2.68	0.06	84.1	200	–	–	400
Mo, μg/L	26.9	<1.0[h]	103	10	–	–	70
Ni, μg/L	3.05	<0.25[h]	2,019	200	–	70	70
Pb, μg/L	1.01	0.01	76.1	5,000	15	10	10
Se, μg/L	7.86	<0.21[h]	80.1	20	50	40	10
U, μg/L	9.18	<0.12[h]	33.9	–	30	30	–
V, μg/L	30.6	<0.24[h]	87.0	100	–	–	–
Zn, μg/L	97.6	<0.49[h]	14,700	2,000	–	–	–

[a]United Nations Food and Agriculture Organization.
[b]US Environmental Protection Agency (USEPA, 2009).
[c]World Health Organization (WHO, 2011).
[d]Gulf Cooperation Council Standardization Organization (GSO, 2008).
[e]Concentrations will cause no restriction to crop growth and health.
[f]Concentrations will cause slight to moderate restriction to crop growth and health.
[g]Concentrations will cause severe restriction to crop growth and health.
[h]Less than instrumental detection limit.

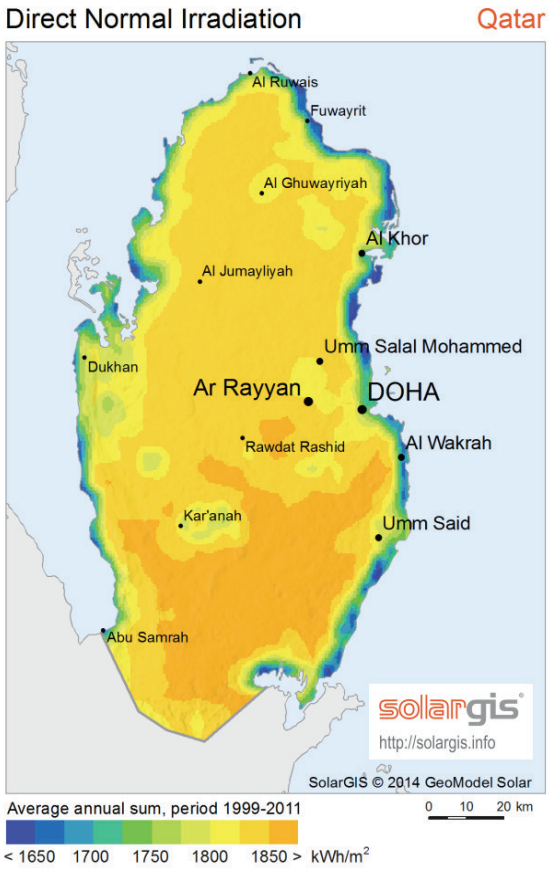

Fig. 3. Qatar average annual direct normal radiation map, generated by SolarGis [6].

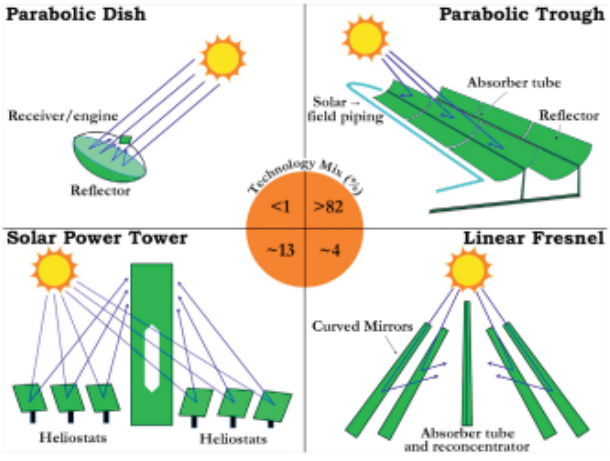

Fig. 4. Various CSP technologies along with their installed ratios [4].

as a renewable energy source with the inherent possibility of including a thermal energy storage subsystem for improving the plant dispatchability. Next generation systems will require higher operating temperatures and larger heat flux densities in an effort for increasing the overall efficiency and reducing specific costs. In that context, advanced HTFs can face those challenges and largely contribute to the economics of future solar thermal systems [8].

3. Agriculture farms water needs

Once plants total growing period is known, the duration (in days) of various growth stages has to be determined [9]. The total growing period is divided into four stages: (i) the initial stage: this is the period from sowing or transplanting until the crop covers about 10% of the ground; (ii) the crop development stage: starts at the end of the initial stage and lasts until the full ground cover has been reached (ground cover 70%–80%), it does not necessarily mean that the crop is at its maximum height; (iii) the mid-season stage: starts at the end of the crop development stage and lasts until maturity; it includes flowering and grain setting; (vi) the late season stage: starts at the end of the mid-season stage and lasts until the last day of the harvest; it includes ripening. Table 4 shows the duration of the various growth stages for some of the major crops. For each crop the "minimum" and "maximum" duration of total growing period have been taken and subdivided to various growth stages. The crop of tomato, for example, has an average water need if compared with other crops, therefore, its water needs is selected in the present study. Table 5 shows the daily water production which calculated based on the maximum average 4.5 mm/d of water need times the areas required for irrigation as a function of the sunny hours per day (7 h) and the total production per day. In the present work, the suggested areas need to be irrigated by the produced water are 40,000, 100,000, 250,000 and 450,000 m^2. Therefore, the daily required water needs to produce by the proposed hybrid desalination system should be 617, 1,543, 3,857 and 6,943 m^3, as shown in Table 5, which calculated based on the maximum value of the average water need in mm/d.

4. Proposed system description

The suggested dual-purpose water/power plant is designed with four unit sizes (base case and three alternatives) to generate electricity and produce water to serve the suggested farm areas that mentioned in Table 5. The farm area of 40,000 m^2 selected to be studied in detail in this work is a typical base case. Fig. 5 shows the process diagram of the base case solar-power-desalination plant to generate 68 kW nominal electrical power and produce water around 618 m^3/d using groundwater with salinity of 15,000 ppm as feedwater to the system.

The solar unit consists of number of LFC modules connected in parallel, driven by pressurized hot water to raise the feedwater temperature of the vacuum multi-effect membrane distillation (V-MEMD) in the brine heater. Part of the pressurized hot water passes out of LFC through another set of parallel number of LFC modules to generate steam at 160°C and 6.1 bar to drive the turbo-generator. Fig. 6 shows a schematic diagram of the three modules of the LFC row, the present study, the LFC row consists of 16 modules, each module (64 m total length and 7.5 m width) generates 12.3 kW thermal power. The turbo-generator system will generate the electrical power to provide the electrical power required to all systems in addition to provide the electricity for the farm community during the day hours. The turbine-exhausted

Table 2
Comparison of major CSP technologies along with operating temperature range [4]

	PTC	SPT	LFC	PDS
Capacity range (MW)	10–250	10–100	5–250	0.01–1
Operating temperature range, °C	150–400	300–1,200	150–400	300–1,500
Solar concentration ratio	50–90	600–1,000	35–170	<3,000
Solar to electricity efficiency, %	10–16	10–22	8–12	16–29
Relative cost	Low	High	Low	Very high
Power cycle	Steam Rankine; organic Rankine	Steam Rankine; Brayton cycle (gas turbine)	Steam Rankine; organic Rankine	Stirling engine; steam Rankine; Brayton cycle (gas turbine)
Commercial maturity	High	Medium	Medium	Low
Outlook for improvements	Limited	Very significant	Significant	High potential through mass production
Advantages	Long-term proved reliability and durability; modular components; compatible with combined cycles burning oil or gas	High efficiency; compatible with Brayton cycle and combined cycles burning oil or gas; modular components	Simple structure and easy construction; modular units; compatible with combined cycles burning oil or gas	High efficiency; modular units; no need for water cooling
Disadvantages	Relatively low efficiency; limited operational temperature; complex structure; need water for cooling and cleaning	High maintenance and equipment costs; need water for cooling and cleaning	Relatively low efficiency; limited operational temperature	Low commercial maturity; no thermal storage available

steam will be condensed using the brine of the reverse osmosis (RO) unit then mix with the hot fluid of the brine heater to circulate into the LFC through a pressure pump.

Each V-MEMD module comprises six multi-effect stages with no steam raising unit and no module condenser. The heated brine at 80°C will be the feedwater required for all V-MEMD modules, while the produced vapor will be condensed in a common final condenser. This final condenser creates the vacuum, which drives the steam flow through the vacuum membrane distillation (VMD) modules. The remaining heat of condenser is released via cooling tower loop. Memsys' V-MEMD achieves high recover ratios with high feedwater salinity, as shown in Fig. 7 [10–12]. Further concentration of RO brine rejected at around 40,000 ppm, the V-MEMD recovery ratio (RR) can be reach up to 70% without any degradation on the membranes. In the present study, V-MEMD unit is designed only with 42% RR. Part of the rejected brine will be recycled to mix with raw feedwater as feedwater to the RO unit, while the other part will be discharged into a solar pond.

The RO unit is designed with 40% RR with a partial blending flow mix with the permeate to increase the salinity to <2,000 ppm for the irrigation use, as the outlet permeate salinity by RO is very low to use for irrigation water. The rejected brine used to condense the turbine-exhausted steam then pass through the brine heater to rise its temperature before feeding the V-MEMD. The hybrid RO/V-MEMD desalination units convert the groundwater into irrigation water and some as potable water. To control final rejected brine salinity to be almost four times of the groundwater salinity, a part of the rejected brine of V-MEMD is recycled into the feed mixer with the raw water to give a constant salinity for RO unit.

Fig. 8 shows the line diagram of the pressurized RO, system comprises of one pass with two stages with energy recovery device and permeate blending flow; each consists of four pressure vessels and six membrane elements in each vessel. The used membranes is SWC4B-LD seawater high salt rejection (99.7%) and membrane size is 8″ × 40″ with 440 ft^2 (40.74 m^2) surface area.

The pretreatment and posttreatment systems are included and operate under commercial conditions. The chlorination dosing system is installed before feed pump to kill any biological species in the feedwater, then the dechlorination dosing system is installed before the fine filter to remove the residual of chlorine. In between, the pretreatment system includes the acid, sodium hypochlorite, antiscalant and sodium bisulfate dosing subsystems. At the end of the process, the caustic soda dosing system, as a posttreatment, will applied to control the pH of the permeate.

Table 3
Thermophysical properties of liquid metals and state-of-the-art heat transfer fluids, all properties at 1 bar, 600°C, [8]

Heat transfer fluid	T_{min}, °C	T_{max}, °C	c_p, kJ/kg K	λ, W/m K	ρ, kg/m^3	μ, mPa s	Cost[a], $/kg
Alkali metals							
NaK eutectic (22.2–77.8 wt% Na–K)	–12	785	0.87	26.2	750	0.18	2
K	64	766	0.76	34.9	705	0.15	2
Na	98	883	1.25	46.0	808	0.21	2
Li	180	1,342	4.16	49.7	475	0.34	60
Heavy metals							
PbBi eutectic (44.5–55.5 wt% Pb–Bi)	125	1,533	0.15	12.8	9,660	1.08	13
Bi	271	1,670	0.15	16.3	9,940	1.17	22
Pb	327	1,743	0.15	18.8	10,324	1.55	2
Fusible metals							
Ga	30	2,237	0.36	50.0	6,090	0.77	600
In	157	2,072	0.24	47.2	6,670	0.75	500
Sn	232	2,687	0.24	33.8	6,330	1.01	25
State-of-the-art HTFs							
Air	n.a.	n.a.	1.12	0.06	0.40	0.03	0
Water/steam	0	n.a.	2.42	0.08	22.1	0.03	~0
Solar salt (60–40 wt% $NaNO_3$–KNO_3)	220	600	1.10	0.52	1,903	1.33	0.5

T_{min} and T_{max} represent the normal melting and boiling points, except for solar salt (chemical stability limit), and gases (n.a. = not available).
[a]Consider commodity prices (commercial purity) as of end of 2012 show large variations and should only as a rough order-of-magnitude approximation.

Table 4
Approximate duration of growth stages for various crops and water needs [9]

Crop	Total duration	Initial stage	Crop development stage	Mid-season stage	Late season stage	Water need, mm/total growing period	Water need, mm/d (average)[a]
	Day						
Bean/green	75	15	25	25	10	300–500	4–5.6
	90	20	30	30	10		
Cabbage	120	20	25	60	15	350–500	2.9–3.6
	140	25	30	65	20		
Maize/sweet	80	20	25	25	10	500–800	6.3–7.3
	110	20	30	50	10		
Melon	120	25	35	40	20	400–600	3.3–3.8
	160	30	45	65	20		
Oats	120	15	25	50	30	450–650	3.8–4.3
	150	15	30	65	40		
Onion/dry	150	15	25	70	40	350–550	2.3–2.6
	210	20	35	110	45		
Pepper	120	25	35	40	20	600–900	5
	210	30	40	110	30		
Potato	105	25	30	30	20	500–700	4.8
	145	30	35	50	30		
Tomato	135	30	40	40	25	400–800	3.0–4.5
	180	35	45	70	30		
Wheat	120	15	25	50	30	450–650	3.8–4.3
	150	15	30	65	40		

[a]Calculated.

Table 5
Daily water production to produce tomato for four suggested farms areas

	Base case	Alternative 1	Alternative 2	Alternative 3
Farm area, m^2	40,000	100,000	250,000	450,000
Water production in m^3/7 h	180	450	1,125	2,025
Water production, m^3/d	617	1,543	3,857	6,943

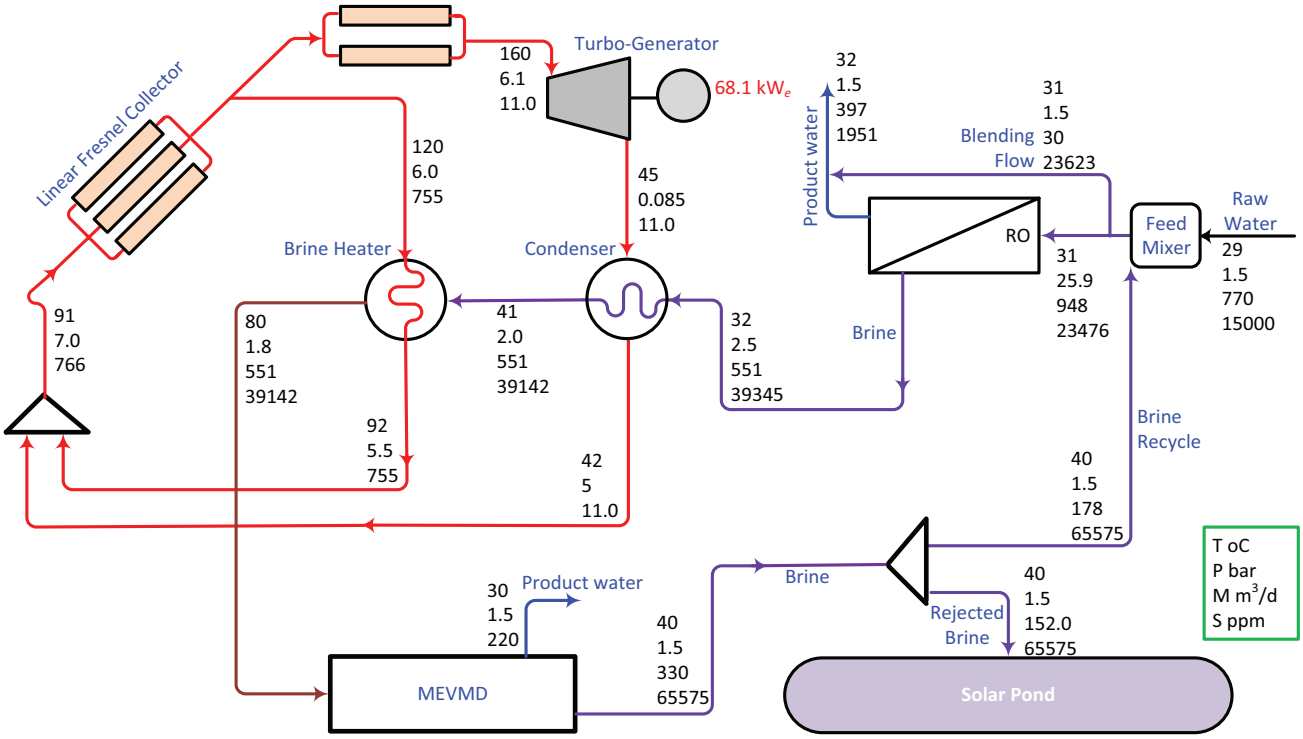

Fig. 5. Solar LFC heat and mass balance of the solar-power-desalination plant (generate 68 kW_e and produce 617 m^3/d).

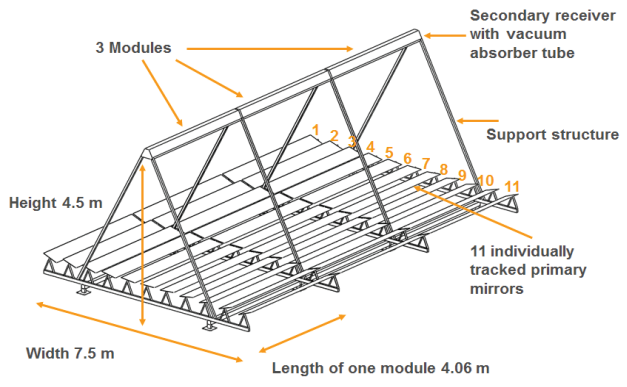

Fig. 6. Schematic diagram of three modules of LFC row.

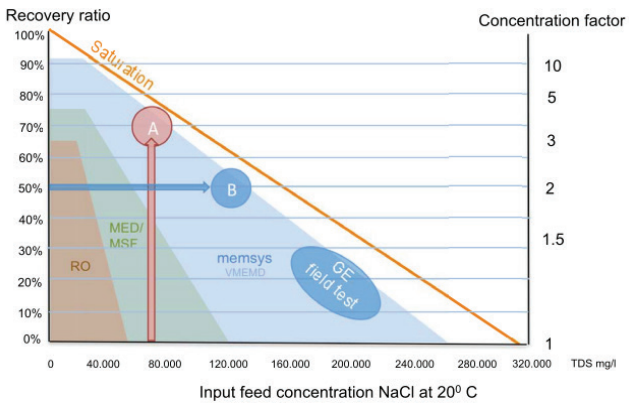

Fig. 7. Memsys achieves recovery rates in brine concentration [10].

Solar pond with liner has several important advantages. They can be built easily and at a relatively low cost over large areas, using and storing solar energy on a grand scale. They cannot pollute the air, and coupled with suggested desalination systems to keep the discharged brine without mixing with groundwater.

5. Mathematical model

5.1. RO governing equations

The osmotic pressure (p) in kPa of a solution is calculated using the experimentally measured concentration of

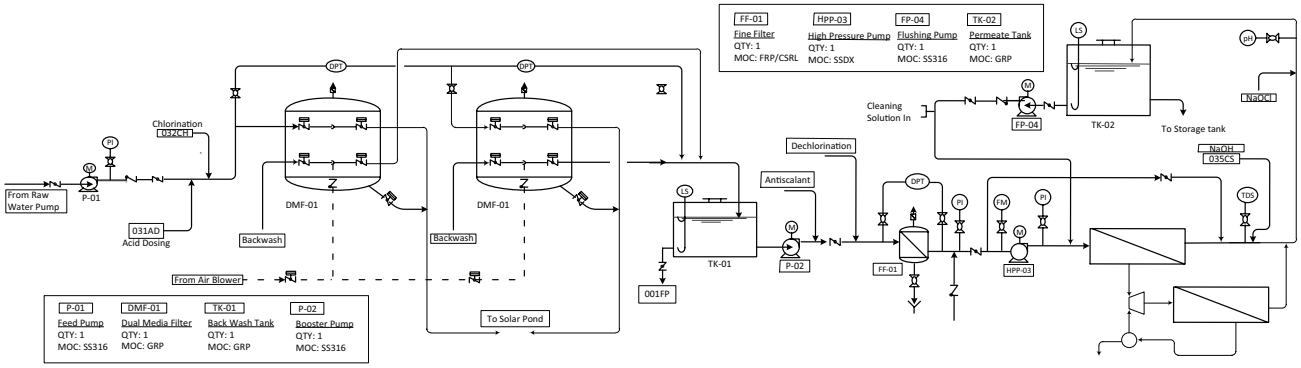

Fig. 8. Flow line diagram of RO unit subsystem.

dissolved salts (ppm) in the solution and can be calculated using Eq. (1).

$$\pi = 7.584 \times X / 1000 \tag{1}$$

where X is the water salinity in ppm. While, salt rejection (SR) is defined by Eq. (2), where S_P and S_F are the permeate and feed salinity, respectively.

$$SR = \left(1 - S_P / S_F\right) \times 100 \tag{2}$$

The following relation, Eq. (3), defines the rate of water passage through a semi-permeable membrane:

$$M_P = \left(\Delta P - \Delta\pi\right) K_W A \tag{3}$$

where M_P is the rate of water flow through the membrane (m^3/s); ΔP and $\Delta\pi$ are net the hydraulic and osmotic pressure differential across the membrane (kPa), respectively; K_W is the water permeability coefficient (m^3/m^2 s kPa) and A is the membrane area (m^2).

$$\Delta P = \overline{P} - P_P \tag{4}$$

$$\Delta\pi = \overline{\pi} - \pi_P \tag{5}$$

where P_P and π_P are the hydraulic and osmotic pressures of permeate, respectively. $\overline{P}$ and $\overline{\pi}$ are the arithmetic average of the hydraulic and osmotic pressures for the feed and brine sides.

5.2. VMD governing equations

For VMD, the vapor transport occurs in three steps: (i) evaporation from the hot saline feed, (ii) vapor transport through the porous membrane and (iii) condensate the transported vapor in outside condenser, which the vacuum is created through a vacuum pump. The temperature difference across the two sides of the hydrophobic membrane leads to a pressure difference that causes water to evaporate. Due to high surface tension of the polymeric membrane materials, liquid water is prevented from entering the membrane pores, while molecular water in the vapor phase can pass through. Eq. (6) represents the transmembrane flux (J_m) along the membrane length. The influence of the pressure conditions across the membrane's surface is more significant on the permeate flux. Eq. (7) represents the conduction heat transfer rate through the membrane material while Eq. (8) used to calculate the total heat transferred by VMD. The membrane surface temperature ($T_{f,m}$) can be determined by the flow bulk temperature and the coefficient of heat transfer, as shown in Eq. (9).

$$J_m = C_m \left(P_{f,m} - P_{\text{vac}}\right) \tag{6}$$

$$q_m = K_{\text{cond}} \left(T_{f,m} - T_P\right) / \delta_m \tag{7}$$

$$q_{\text{out}} = J_m h_{g,f} + q_m \tag{8}$$

$$T_{f,m} = T_{f,b} - q_{\text{out}} / h \tag{9}$$

5.3. LFC governing equations

The solar cycle, which comprises of a set of LFC modules, turbo-generator, condenser and a pressurized pump. A set of LFC modules will generate hot pressurized water and another set will generate a saturated steam. The saturated steam will enter the turbine to drive it while the exhausted steam exits the turbine at condenser temperature. The following equations describe how to calculate the power generated by the turbine:

$$x_2 = \left(S_1 - S_{f,3}\right) / \left(S_2 - S_{f,3}\right) \tag{10}$$

$$h_2 = h_{f,3} + x_2 \left(h_{g,2} - h_{f,3}\right) \tag{11}$$

$$\eta_{\text{isoentropic}} = \left(h_1 - h_{g,2}\right) / \left(h_1 - h_2\right) \tag{12}$$

$$\text{Pump input} = v_{f,3}\left(P_1 - P_2\right) = h_4 - h_3 \quad (13)$$

$$\text{Net work out} = \dot{m}\left[\left(h_1 - h_2\right) - \left(h_4 - h_3\right)\right] \quad (14)$$

$$\text{Heat needed to evaporate the water by LFC} = \dot{m}\left(h_1 - h_4\right) \quad (15)$$

6. Model results and discussion

The overall base case system simulated using Aspen Plus V8.8 – aspenONE, as shown in Fig. 9. The simulation of coupling all subsystems results the distributions of the temperature, pressure, flow rate, vapor fraction, power consumption and electrical power production. The first row of LFC pumped into the absorbers with pressurized water at 91°C and 7 bar with 766 m^3/d, then after gaining the solar energy the pressurized water increases its temperature up to 120°C. Part of 755 m^3/d is used in the brine heater to rise the RO rejected brine temperature up to 80°C and the pressurized water then cooled at 92°C. The other part (rated 11 m^3/d) of first row of LFC outlet will pass through the second set of LFC to gain additional solar energy to generate saturated steam at 160°C to drive the turbo-generator and produce 68 kW electrical powers. The exhausted steam exits at 45°C then condensed in the condenser and pumped to 5 bar to mix with the first part and both are recirculated in solar LFC cycle. The turbine's isentropic efficiency is 90% while the mechanical efficiency can reach to 95%.

Fig. 10 shows the sensitivity analysis of the turbine operation parameters; temperature, pressure and mass flow rate as a function of generated power. The maximum generated power as a function of applied temperature at 320°C reached to 109.4 kW (Fig. 10(a)), while with 40 bar applied pressure reached to 98.8 kW, as shown in Fig. 10(b). However, increasing the flow rate of the pressurized LFC pump at operating conditions of 160°C and 6.1 bar, the maximum electrical power generated by turbo-generator at nominal operating conditions can reach to 84 kW, which is limited by the vapor fraction of the condensed exhausted steam in the condenser. Meanwhile at the available LFC maximum operating allowable pressure (40 bar) and the saturation temperature at 250°C, the generated power can increase with increasing the flow rate until 125 kW at 14 m^3/d flow rate, as shown in Fig. 10(c).

Fig. 11 shows the RO rejected brine of the first stage is at pressure 18.9 bar will passes through energy recovery turbine (ERT) to pump at 29.1 bar into the second stage of RO modules while the turbo boost pressure reached to 10.5 bar. ERT saves about 53.2% of the required energy. Fig. 11 shows the base case results using the integrated membrane solution design (IMSDesign-2016), Version: 1.215.1602.24.69% [13]. The changes in TDS from point 1 to point 4 are due to the pretreatment process and adding some chemical materials.

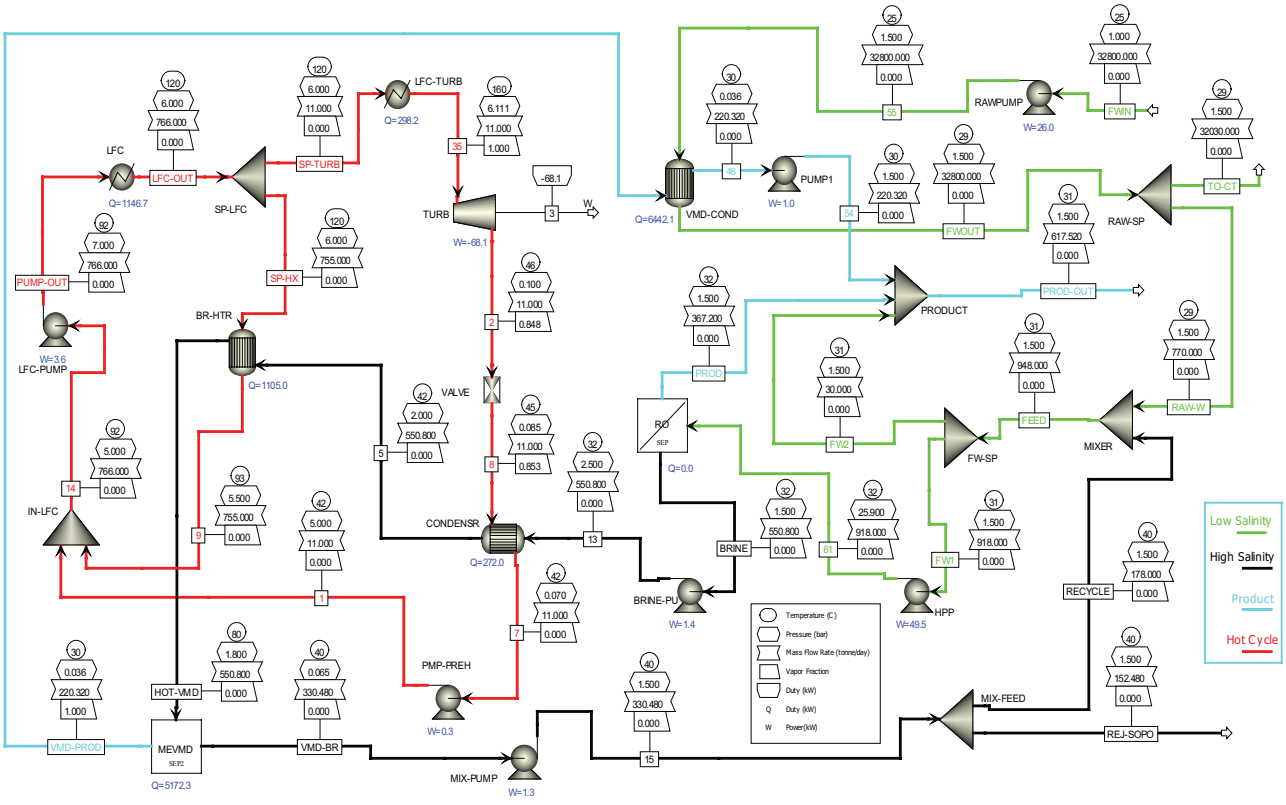

Fig. 9. Aspen simulation model result of solar-power-desalination plant.

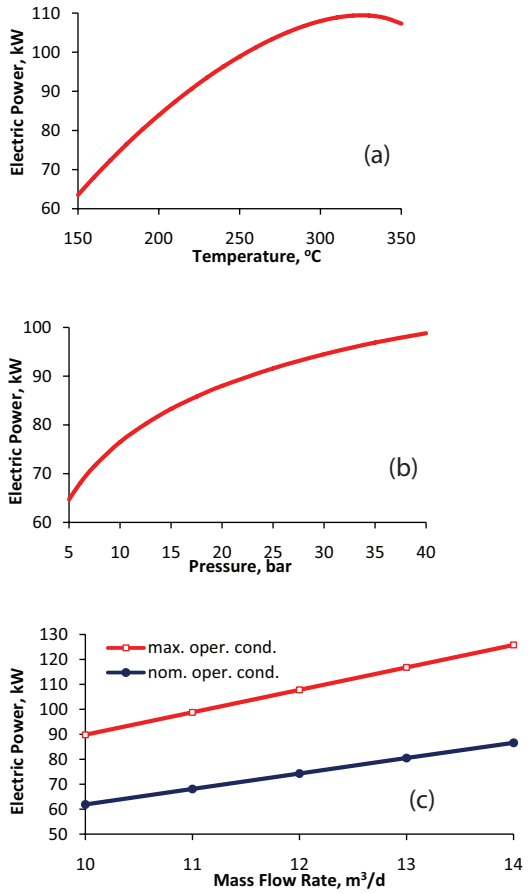

Fig. 10. Effect of operating parameters of the steam turbine on the generated electric power (a) steam temperature, (b)steam pressure and (c) mass flow rate.

The RO base case system is designed with 40% RR for two stages to give 391.2 m^3/d permeate production. The system is designed with raw water of a well at high-level TDS of 15,000 ppm and 770 m^3/d flow rate. The raw water will be mixed with 178 m^3/d recycled flow rate of the discharged brine of V-MEMD at TDS 65,575 ppm to give feedwater for RO modules at 948 m^3/d with 23,476 ppm salinity. Therefore, the used feedwater salinity for the RO unit designed at TDS of 23,476 ppm and to adapt the salinity required for irrigation purpose. 30 m^3/d blending flow of feedwater will be mixed with the RO permeate (at TDS 169 ppm) to give TDS irrigation water 1,976 ppm. The final salinity due to mixing the permeate of RO unit with V-MEMD will be 1,271 ppm to store into the product tank.

Fig. 12 indicates the pressure reduction in pass-1 due to increasing the feedwater temperature and consequently indicated the specific pumping energy due to the same reason. At the same test value of the previous figure, the RO module behavior indicates in Fig. 13, at which the permeate salinity will be decreased while the brine salinity will be increased due to increasing the feedwater temperature.

The V-MEMD unit installed to recover additional freshwater from the RO rejected brine after heating it in the brine heater. The flow rate of the V-MEMD rejected brine increases with increasing the RO brine salinity of the RO unit, as shown in Fig. 14. At the same time, the recycled flow to mix with the raw water will be decreased to keep the output TDS at constant value of 23,475 ppm. The designed RR of V-MEMD is 42%, which it convert 220 m^3/d freshwater from 550.8 m^3/d feedwater. Therefore, system RR will be 80.1%.

Table 6 summarizes the main technical specification of the cogeneration solar dual-purpose plant using solar LFC

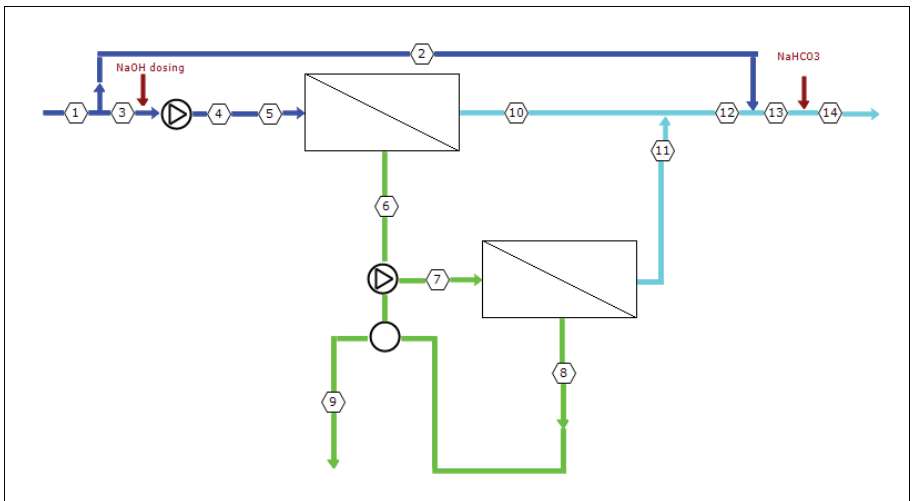

	1	2	3	4	5	6	7	8	9	10	11	12	13	14
Flow rate, m^3/d	928.8	30	900	900	900	775.2	775.2	540	540	124.56	235.92	360	391.2	391.2
Pressure, bar	0	0	0	19.7	19.7	18.9	29.1	28.5	0.3	0	0	0	0	0
TDS, ppm	23476	23659	23659	23660	23660	28625	28625	39345	39345	210	147	169	1974	1976
pH	6.99	6.99	6.99	7.60	7.60	7.61	7.61	7.68	7.68	6.43	6.39	6.41	6.84	7.1
SDSI	-1.02	-1.02	-1.02	-0.40	-0.40	-0.29	-0.29	-0.07	-0.07	-5.50	-5.92	-5.75	-3.17	-2.65

Fig. 11. Flow analysis of two-stage SWRO (consists of five pressure vessels and four elements per each) to produce 391.2 m^3/d permeate flow with 40% recovery ratio and 53.2% energy recovery turbine.

and hybrid RO/V-MEMD desalination plant. Depending on the required irrigation land and the average water required to produce tomato, the total water production per each desalination system are calculated for the four designs. The total percentage area required to install the suggested dual-purpose plants vs. the total farms' land are 9.3%, 8.5%, 8.0% and 7.8% for the farms of base case 1, case 2, case 3 and case 4, respectively, as shown in Fig. 15.

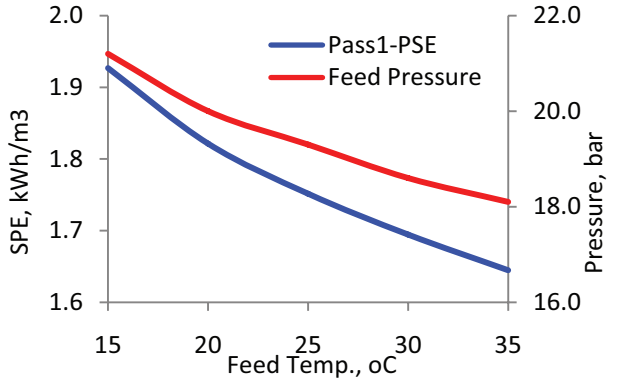

Fig. 12. Feedwater temperature vs. pass-1 pumping specific energy and feed pressure.

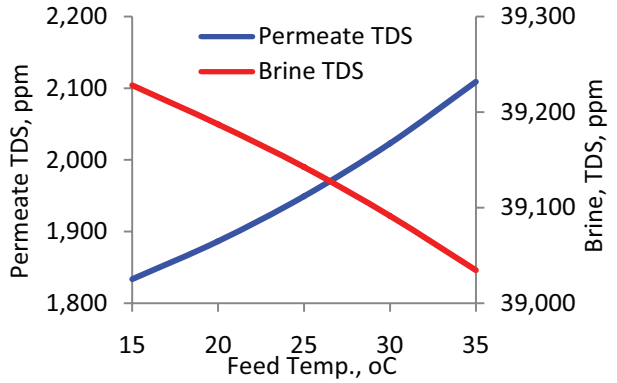

Fig. 13. Feedwater temperature vs. pass-1 TDS of permeate and brine.

7. Conclusions

The suggested solar-power-desalination plants can achieve goal points as follows:

- This work presented a small-scale solar-power-desalination (base case) plant to generate electricity and produce desalinated freshwater. The integrated system is designed to provide the optimum solution for big desert farms of high groundwater salinity (of 15,000 ppm and more), which RO units is designed with 40% recovery and its brine is used to feed V-MEMD units to recover 42% from the RO brine.

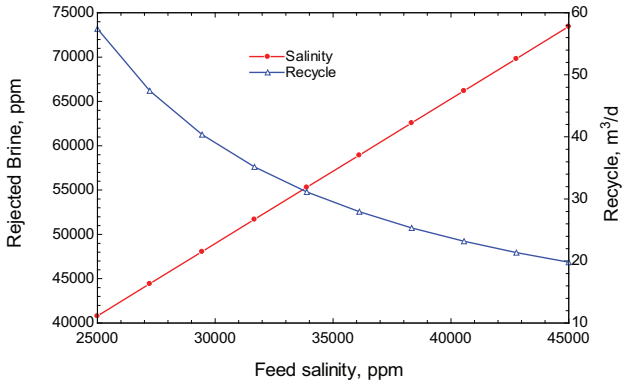

Fig. 14. Effect of V-MEMD feedwater salinity on the brine salinity and recycle flow rate.

Table 6
Summary of specifications of solar dual-purpose systems at different designs

	Case 1 (base case)	Case 2	Case 3	Case 4
RO unit production, m^3/d	398	998	2,488	4,490
V-MEMD unit production, m^3/d	220	551	1,332	2,398
Total water production, m^3/d	618	1,549	3,861	6,968
Raw water, m^3/d	770	1,926	4,874	8,800
Permeate blending, m^3/d	30	79	199	360
Brine disposal into solar pond, m^3/d	152	377	1,013	1,830
Solar LFC heating water, m^3/d	755	1,888	4,717	8,490
Solar LFC heating steam, m^3/d	11	22	38	50
Electric power, kW	68	136	235	310
# of Solar LFC first group	6	16	40	74
# of Solar LFC second group	2	3	6	7
# of RO first stage (pressure vessel × elements)	4 × 6	6 × 6	14 × 6	25 × 6
# of RO second stage (pressure vessel × elements)	4 × 6	5 × 6	12 × 6	20 × 6
# of V-MEMD modules	32	78	192	345
Area of solar/desalination field, m^2	4,545	10,215	23,785	41,343
Irrigation land, m^2	40,000	100,000	250,000	450,000

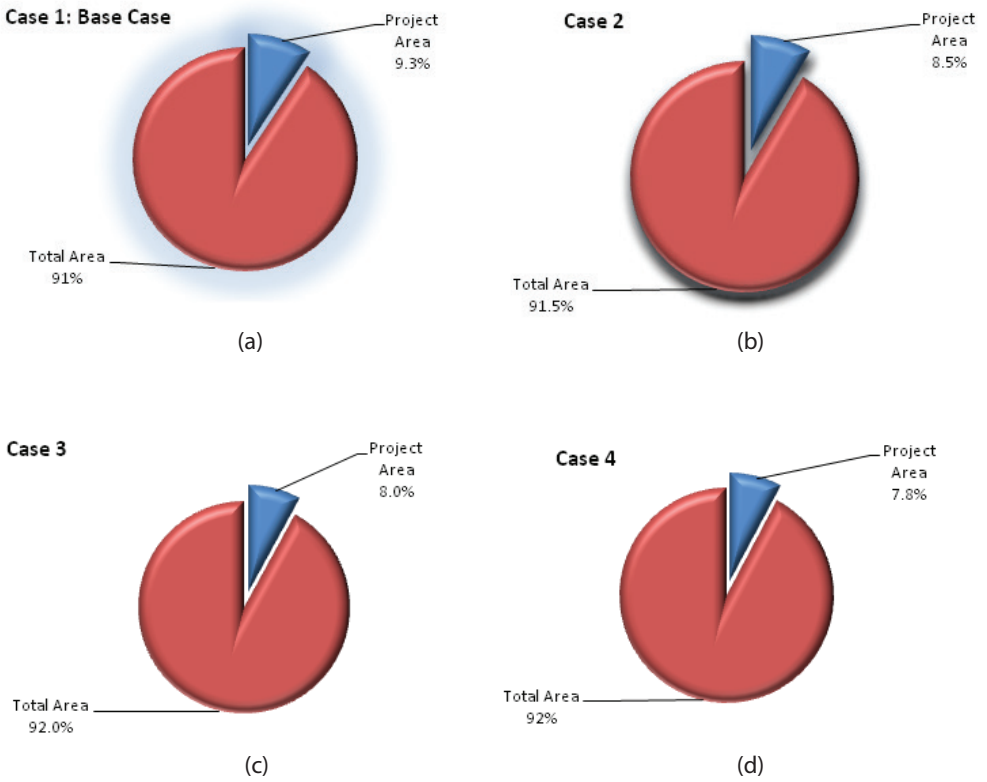

Fig. 15. Comparison land required for the project engineering vs. total farms' land.

- The base case is designed to provide the plant and the farm with electrical power (rating 68 kW) while the hybrid desalination plant is designed with 617 m^3/d capacity. The electric power can be reach to 125 kW by increasing the flow rate of LFC with the same other operating conditions.
- Other scale up designs for electricity and water production are indicated.
- Maximize the utilization of the new technology to cultivate the desert lands that far from the required resources of water and electricity.
- The project could be a core for several research points with the academic institutions with no effect on the project production.
- The technical production project's area decreases with increasing the irrigated farm's land.
- The project RR will be increased if the farm groundwater has lower salinity than that mentioned in the study.

Acknowledgments

This was made possible by NPRP grant # NPRP9-028-2-012 from the Qatar National Research Fund (a member of Qatar Foundation). The findings achieved herein are solely the responsibility of the authors.

References

[1] Economist Intelligence Unit, The GCC in 2020: Resources for the Future, 2010.
[2] B. Wire, Qatar Water Report Q3 2010, 2010 [Online]. Available at: http://www.businesswire.com/news/home/201009130065
[3] N. Kuiper, C. Rowell, B. Shomar, High levels of molybdenum in Qatar's groundwater and potential impacts, J. Geochem. Explor., 150 (2015) 16–24.
[4] X. Xu, K. Vignarooban, B. Xu, K. Hsu, A.M. Kannan, Prospects and problems of concentrating solar power technologies for power generation in the desert regions, Renew. Sustain. Energy Rev., 53 (2016) 1106–1131.
[5] M. Balghouthi, S.E. Trabelsi, M. Ben Amara, A.B.H. Ali, A. Guizani, Potential of concentrating solar power (CSP) technology in Tunisia and the possibility of interconnection with Europe, Renew. Sustain. Energy Rev., 56 (2016) 1227–1248.
[6] SolarGis, Solar Radiation Maps, 2016 [Online]. Available at: http://solargis.info/doc/free-solar-radiation-maps-DNI#Q (Accessed May 2016).
[7] Y. Tian, C.Y. Zhao, A review of solar collectors and thermal energy storage in solar thermal applications, Appl. Energy, 104 (2013) 538–553.
[8] J. Pacio, T. Wetzel, Assessment of liquid metal technology status and research paths for their use as efficient heat transfer fluids in solar central receiver systems, Sol. Energy, 93 (2013) 11–22.
[9] CDR FAO, Calculation of the Crop Water Need. Available at: http://www.fao.org/docrep/s2022e/s2022e07.htm#3.3
[10] Memsys Thermal Separation Process, FAQ-Frequently Asked Questions: The Memsys Process of Thermal Membrane Distillation.
[11] The Memsys Process, 2015. Available at: www.memsys.eu, Memsys_datasheet_4_6_4 2015-02
[12] The Memsys Process, 2016. Available at: www.memsys.eu, Memsys_datasheet_6_52_2016_09
[13] Hydranautics Nitto Group Company, IMSDesign-2016 Software, 2016.